# Metallo-Dielectric Photonic Crystals for Surface-Enhanced Raman Scattering

**Yu Zhao,[†] Xue-Jin Zhang,[†] Jing Ye,[‡] Li-Miao Chen,[†] Shu-Ping Lau,[‡] Wen-Jun Zhang,[†] and Shuit-Tong Lee[†,*]**

[†]Center of Super-Diamond and Advanced Films (COSDAF) and Department of Physics and Materials Science, City University of Hong Kong, Hong Kong SAR, China, and [‡]Department of Applied Physics, Hong Kong Polytechnic University, Hong Kong SAR, China

**ABSTRACT** Metallo-dielectric photonic crystals (MDPCs) are used as ultrasensitive molecular detectors for concentrations down to picomolar level based on surface-enhanced Raman spectroscopy (SERS). Calculations show that the amorphous silicon photonic crystals (a-Si PCs) embedded in multiple metallo-dielectric (MD) units can significantly increase the electromagnetic fields at the air–dielectric interface, leading to remarkable Raman enhancement. Corresponding experiments show the multiple MDPC structures can serve as an ultrasensitive SERS substrate with excellent reproducibility and stability, capable of quantitative analysis down to 10 pM level. The MDPC structure can be generalized to other applications, such as plasmonic devices, ultrasensitive sensors, and nanophotonic systems.

**KEYWORDS:** silicon · metallo-dielectric · electromagnetic field · template synthesis · SERS

Since the discovery in the 1970s that the Raman signals of adsorbates on a roughened silver electrode can be greatly enhanced by a factor of $10^5$–$10^6$,[1–3] surface-enhanced Raman scattering (SERS) has been attracting increasing interest for basic research as well as a powerful spectroscopic technique for ultrasensitive identification of analytes down to single-molecule level.[4,5] Coupled nanoparticles with close spacing and sharp tips or curvatures can have highly concentrated electromagnetic (EM) fields associated with strong localized surface plasmon resonance, which would contribute to substantial Raman enhancement. Consequently, control of the shape, orientation, and self-assembly of nanoparticles is a major focus in current SERS studies.[6–9] One key challenge is to increase the volume fraction of the "hot-spot" region in the entire system, which generally is low and difficult to produce or predict reliably,[10] which may lead to poor reproducibility of Raman signals. Other strategies for surface patterning of periodic noble metal nanostructures are also effective in improving SERS reproducibility,[11–14] although better control of particle size and density and dielectric properties of the surrounding medium are still needed for optimizing the EM characteristics on the surface.[15,16] On the whole, a precisely controlled pattern with submicrometer periodicity on a surface with tunable EM characteristics is needed for practical SERS applications.

In this study, we use a simple method to enhance the surface EM field *via* unique metallo-dielectric (MD) structures designed for ultrasensitive SERS sensing. Our calculations show that the EM field can be greatly enhanced at the air–dielectric interface if multiple MD units are introduced. The MD structure is supported by amorphous silicon (a-Si), and each MD unit is composed of silver and a-Si layer as summarized in Figure 1A, dissimilar to the conventional schemes using sharp metallic tips or closely packed metal particles to create enhanced local field at their vicinity.[17–20] Figure 1B–E shows the distribution of normalized pump irradiance ($I_p$) at 633 nm wavelength through the MD structures with different configurations. The values of pump irradiance $I_p$ are normalized to that of pure a-Si. On the outermost surface, the normalized $I_p$ is 3.4, 6.5, 7.9, and 8.4 for the structure composed of 1, 2, 3, and 4 MD units, respectively. The normalized $I_p$ at the air/a-Si interface reaches saturation for 4 and higher number of units (Supporting Information S1). Figure 1F summarizes the dependence of normalized $I_p$ on MD unit numbers. The calculation clearly shows that the EM field can be greatly enhanced on the proposed MD structures. On the basis of these results, we further combine such MD structures on a substrate with long-range order to form MDPCs.

## RESULTS AND DISCUSSION

Figure 2 shows the schematic illustration and corresponding SEM observations of the fabrication procedures of MDPCs. The PS

* Address correspondence to apannale@cityu.edu.hk.

Received for review January 11, 2011 and accepted March 28, 2011.

**Published online March 28, 2011**
**10.1021/nn2001068**

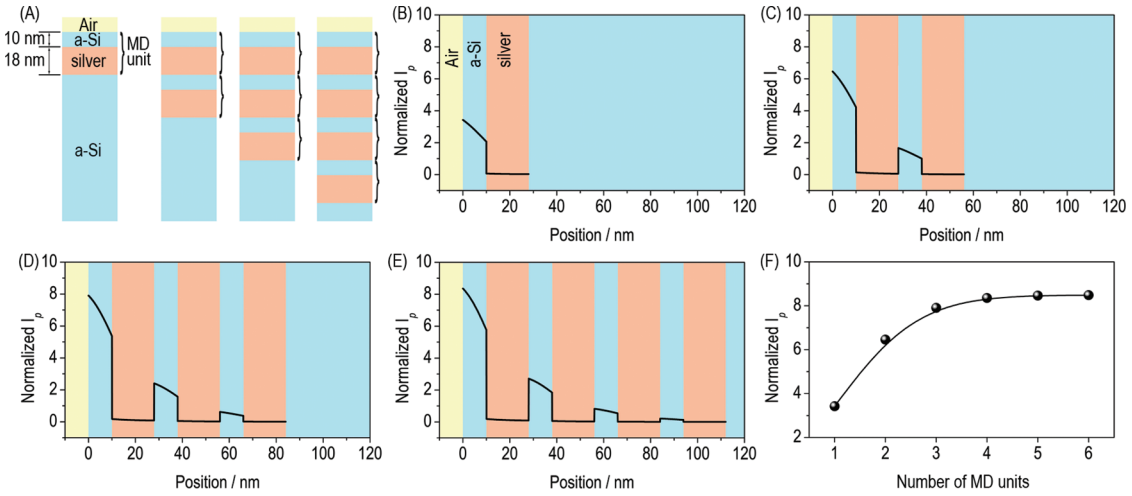


**Figure 1. (A) Schematic illustration of the proposed model of MDPCs. (B–E) Normalized $I_p$ distribution across MDPC structures with 1–4 MD units, respectively. (F) Normalized $I_p$ *versus* the number of MD units.**

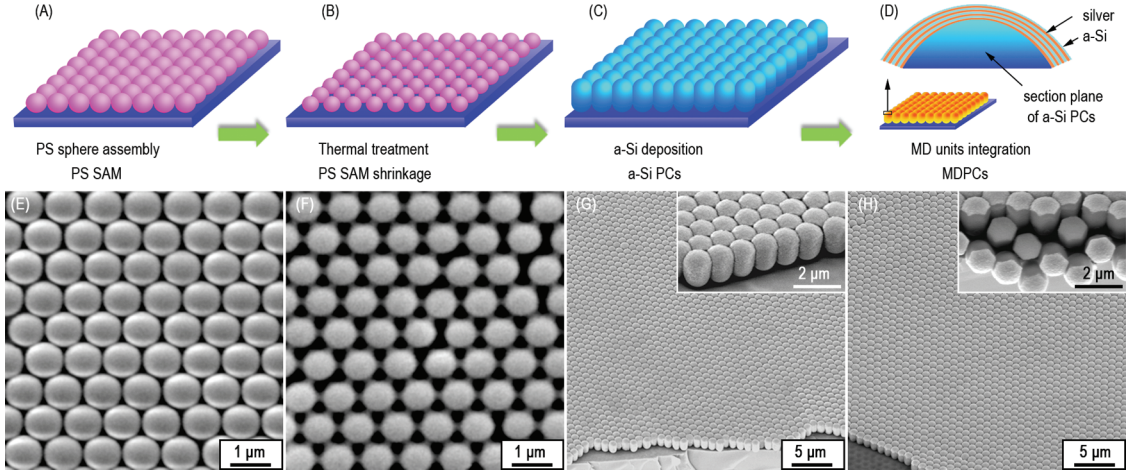


**Figure 2. Fabrication procedures of MDPCs: (A) PS SAM deposited on a supporting substrate; (B) PS SAM shrinkage after thermal treatment; (C) a-Si sputtered onto the PS SAM to form a-Si PCs; (D) MD units integrated into a-Si PCs to form MDPCs. SEM images showing the (E) PS SAM, (F) PS SAM after thermal treatment, (G) a-Si PCs (45° tilted), and (H) MDPCs with 4 MD units (45° tilted). The insets in panels G and H are magnified SEM images showing the rounded-off and sharpened particles of a-Si PCs and MDPCs, respectively.**

SAM was first obtained through our modified self-assembly technique as indicated in Figure 2A. The PS SAM shows ordered hexagonal arrangement, and the diameter of the PS spheres is 978 ± 32 nm, as shown in Figure 2E. Notably, the obtained PS SAM through our modified self-assembly technique almost completely covered the supporting substrate (Supporting Information S2). Also, this technique is applicable to wide-ranging permutations of insulating and conducting flat surfaces regardless of hydrophilic or hydrophobic surface of the supporting substrates. Afterward, to enhance PS SAM mechanical strength and a-Si filling, thermal treatment was applied to the PS SAM as shown in Figure 2B. After the thermal treatment, the diameter of PS spheres was about 800 nm, yielding an average shrinkage of ~18% as observed in Figure 2F. The thermal-treated PS SAM possessed the same alignment with the PS SAM, with very few dislocations and cracks. A thin layer of a-Si was sputtered onto the thermal-treated PS SAM to form a-Si PCs as presented in Figure 2C. SEM observation in Figure 2G confirmed that the obtained a-Si PCs inherited perfectly the ordered hexagonal arrangement and the monolayer integrity. The individual particle is spheroid-like with rough surfaces. The aspect ratio of the individual particle is approximately 2.2:1 and can be well-tuned by controlling the sputtering time. Finally, silver and a-Si are alternately and sequentially sputtered onto the a-Si PCs to form MDPCs with desired MD configurations simply by controlling the sputtering time. Figure 2D schematically summarizes the structural information of a section plane of a-Si PCs containing 4 MD units. For better clarification, the SEM image of a-Si PCs integrated with MD units is given in Figure 2H.

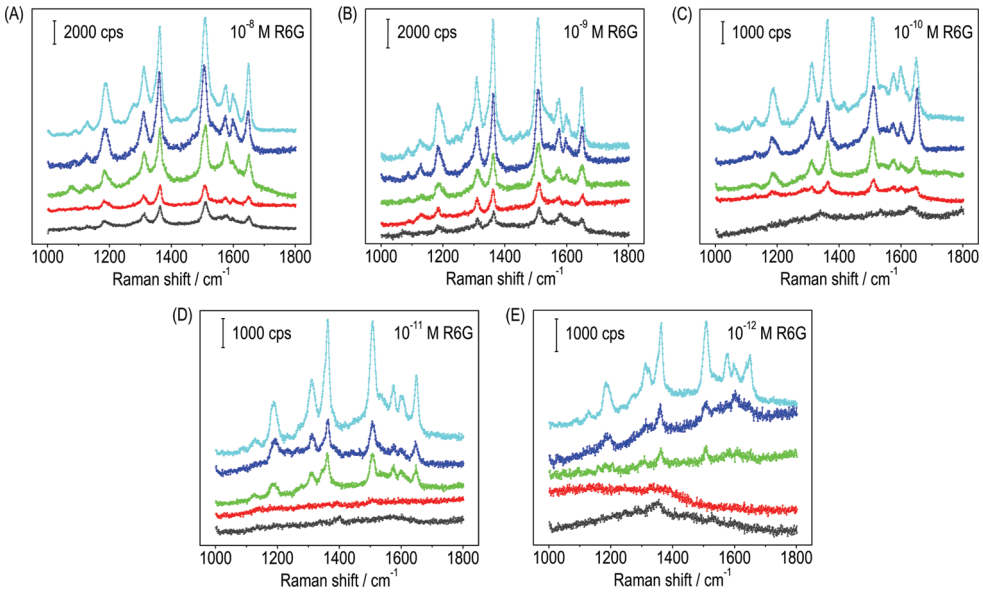


**Figure 3. (A–E) Raman spectra recorded from MDPCs with $C_{R6G}$ decreasing from $10^{-8}$ to $10^{-12}$ M. The spectra in each diagram correspond to MDPCs with one (red), two (green), three (blue), and four (cyan) MD units, respectively. The dark gray curves are obtained from the reference substrates.**

The morphology, dimension, and structure of MDPCs retain the same shape except for the sharpened edges and corners (see Supporting Information S3 for more details).

The lithography-based method allows the preparation of ordered SERS substrates with nanostructures having a wide diversity of shapes and geometries. Our method provides an alternative for achieving precisely controlled spacing, although it remains a challenge to routinely obtain a spacing of less than 10 nm for maximal electromagnetic coupling.[25] The major advantage of the current MDPCs is their high sensitivity down to picomolar level detection of probe molecules owing to the enhanced EM fields and unique wafer-scale platform. To evaluate this capability, SERS spectra were taken from the MDPCs with different MD units using R6G as the probe molecule. Figure 3A–E shows the Raman spectra recorded from MDPCs with R6G concentration ($C_{R6G}$) decreasing from $10^{-8}$ to $10^{-12}$ M. The spectra in each diagram represent the MDPCs with 4 to 1 MD units from top to bottom, respectively, while the bottom dark gray spectra are the reference substrates obtained by directly sputtering a thin silver layer onto the PS spheres. All of the Raman bands match well with the characteristics of the Raman spectrum of R6G.[26] The bands at 1126 and 1188 $cm^{-1}$ are assigned to the C–H in-plane bending mode. The bands at *ca.* 1362, 1509, 1580, and 1649 $cm^{-1}$ are assigned to the C–C stretching modes. It is clear that, for a given $C_{R6G}$, the MDPCs with multiple MD units show stronger Raman signals than the reference ones, and the MDPCs with 4 MD units show the strongest intensity in accordance with our calculation. Significantly, Figure 3 shows that the detection limits of MDPCs with multiple MD units can reach picomolar or lower level, which is more sensitive than the reported detection limits on SERS substrates with long-range periodicity.[27–30]

We suppose that the Raman enhancement is primarily attributed to the MD structure rather than to the coupling of silver nanoparticles or molecular diffusion. On one hand, the experimental data indicate that the Raman intensity or detection limit of MDPCs with 4 MD units is at least 2 orders of magnitude higher than that with 1 MD unit. If the Raman enhancement is primarily due to coupling of nanoparticles in the silver layer, all of the substrates are expected to have similar enhancement because their surface structure is only slightly changed under the same experimental conditions. On the other hand, for a given concentration, the molecular adsorption/desorption and diffusion near the surface region should be the same and contribute the same to Raman signal intensity. However, the experimental results clearly show that the Raman intensities are orders of magnitude different for MDPCs with different MD units. Therefore, we conclude that Raman enhancement should be mainly attributed to the coupling of MD units. The Raman signals in Figure 3E show that the detection limit of R6G on MDPC with 4 MD units is at least $10^{-12}$ M. Assuming all of the molecules in 0.5 mL of R6G solution of $10^{-12}$ M are adsorbed evenly on the $\sim 10^7$ particles in the $3 \times 3$ mm area of MDPCs, we calculate on the average that there are ~30 molecules on each particle. It means that, if the number of molecules surpasses 30 on an individual particle or ~125 molecules within the laser spot area (2 $\mu$m in diameter), the probe molecules would be detectable. This value is comparable to or even better

**TABLE 1. EF and SNR of R6G Molecules ($10^{-10}$ M) on MDPCs with Different MD Configurations**

| number of MD units | EF[a] | SNR |
|---|---|---|
| 1 | $0.21 \times 10^6$ | 6.4 |
| 2 | $0.58 \times 10^6$ | 14.6 |
| 3 | $0.92 \times 10^6$ | 17.8 |
| 4 | $1.5 \times 10^6$ | 23.3 |

[a] EF values are normalized to that of a-Si PCs (see Supporting Information S3).

**TABLE 2. EF and SNR of MDPCs with 4 MD Units at Different $C_{R6G}$**

| $C_{R6G}$ (mol/L) | EF[a] | SNR |
|---|---|---|
| $10^{-8}$ | $3.2 \times 10^4$ | 29.4 |
| $10^{-9}$ | $3.1 \times 10^5$ | 27.1 |
| $10^{-11}$ | $1.2 \times 10^7$ | 20.4 |
| $10^{-12}$ | $0.76 \times 10^8$ | 16.4 |

[a] EF values are normalized to that of a-Si PCs.

than the reported detection limits achieved using surface-enhanced resonance Raman scattering.[31−33]

Furthermore, we investigated the enhancement factor (EF) and noise-to-signal ratio (SNR) of MDPCs. For the estimation of EF, the intensity of the characteristic 1509 $cm^{-1}$ peak was chosen in the expression

$$EF = [I_{SERS}]/[I_{normal}] \times [N_{normal}]/[N_{SERS}] \quad (1)$$

where $I_{SERS}$ and $I_{normal}$ correspond to the normal and SERS signal intensities, respectively,[34] and $N_{normal}$ and $N_{SERS}$ are the number of molecules probed in a bulk sample and that adsorbed on MDPCs, respectively. For the estimation of SNR, the same 1509 $cm^{-1}$ peak was chosen, and calculated according to

$$SNR = 10 \log(I_{signal}/I_{noise})^2 \quad (2)$$

where $I_{signal}$ and $I_{noise}$ are for the intensities of signal and background noise, respectively. For quantitative purpose, the ratio of $I_{signal}$ and $I_{noise}$ should be larger than 10 (equal to SNR > 20).[35] The calculated EF (Supporting Information S4) and SNR values for R6G on MDPCs with different MD units are given in Table 1. As the MD units in MDPCs increased from 1 to 4, the number of R6G molecules adsorbed on a unit area of MDPCs would be slightly changed as mentioned before. However, the EF values increased from $0.21 \times 10^6$ to $1.5 \times 10^6$, and the SNR values decreased from 23.3 to 6.4, correspondingly, according to the SERS spectra. The MD unit configuration not only plays a key role in the enhancement effects but also reveals the potential for quantitative analysis. Table 2 gives the EF and SNR of MDPCs containing 4 MD units. It shows that, at 10 pM $C_{R6G}$, MDPCs with 4 MD units exhibit an excellent SNR of 20.4. The EF increases dramatically as probe molecule concentration decreases, as shown in Figure 4. At high analyte concentration, not all of the target molecules would likely adsorb onto the SERS substrate to

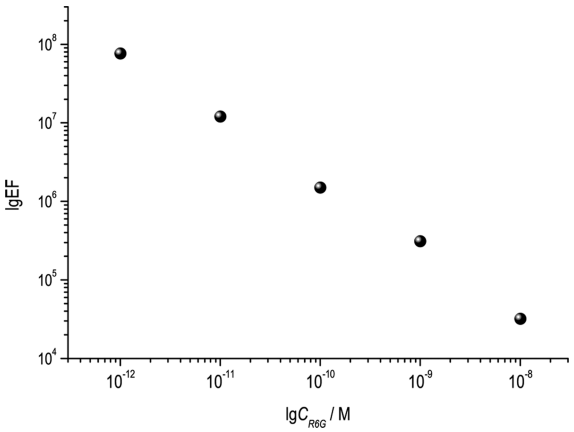


**Figure 4. Enhancement factor (EF) of R6G molecules on MDPCs with 4 MD units at different $C_{R6G}$.**

yield enhanced Raman signals as compared to low concentration, thus the EF would appear higher for the low concentration sample. The calculated logarithmic value of EF is proportional to $C_{R6G}$. It indicates that the EF can be estimated at a given analyte concentration, suggesting MPDCs are highly attractive substrates for quantitative purposes. It is worth pointing out that the calculated EF values are normalized to that of a-Si PCs, which means that the actual EF values are obviously higher than that using bulk R6G as probe molecules because a-Si PCs already possessed remarkable Raman enhancement (Supporting Information S4). Note that the MDPCs also exhibit large Raman enhancement for other probe molecules; for example, the detection limit for 4-MBA is as low as 10 nM level using the MDPCs with 4 MD units, while it is merely at millimolar level in previously reported values[36−38] (Supporting Information S5).

Besides large Raman enhancement and the capability of quantitative analysis, another important advantage of the MDPCs is the homogeneous site enhancement distribution over centimeter-scale area without loss in structural uniformity, yielding improved reproducibility of Raman signals. Figure 5A shows the SERS spectra recorded at 30 randomly chosen spots on MDPCs with 4 MD units. The spot-to-spot intensity variations of the characteristic 1509 $cm^{-1}$ peak are quantitatively displayed in Figure 5B, which shows that 20 of the total 30 data points exhibit an intensity variation within 5%, while the remaining 10 points are within 10%. A recent study showed that silver-coated close-packed PS spheres possessed a broad site enhancement distribution and an extremely low fraction ($\sim 10^{-6}$) of hot-spot sites with an enhancement factor $>10^9$.[10] We also examined the SERS intensity map of MDPCs with different MD configuration at 1 nM $C_{R6G}$ (Supporting Information S6), and the results indicated that as the number of MD units increase, both the sensitivity and the uniformity of SERS signal are greatly improved. The present MDPCs with 4 MD

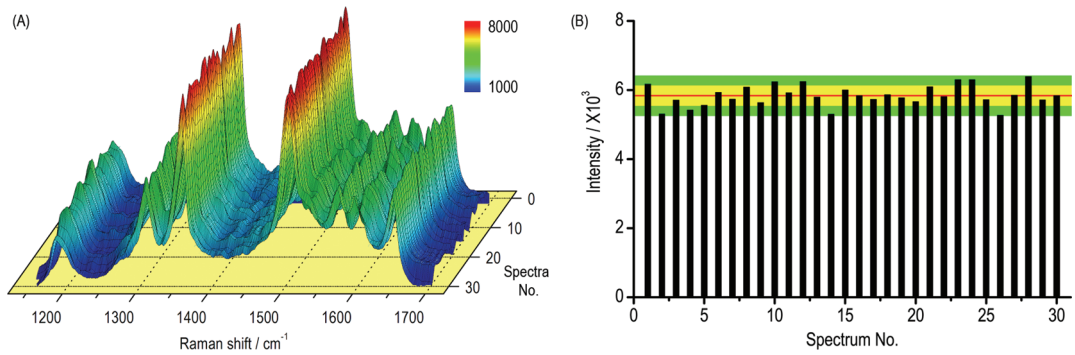


**Figure 5. (A) Reproducibility of Raman spectra on MDPCs with four MD units. Thirty Raman spectra between 1150 and 1700 $cm^{-1}$ were collected at $C_{R6G}$ of $10^{-9}$ M. Colors are assigned according to the relative intensity of the spectra. (B) Intensity distribution of the 1509 $cm^{-1}$ peak in the 30 spectra. The average intensity is indicated with a red line, and the yellow and green zones represent ±5 and ±5−10% intensity variation, respectively.**

units produce much more homogeneous SERS signals, and the enhancement distribution is limited to a relatively narrow region, which is advantageous for quantitative analysis purposes. Besides, the Raman enhancement factor is orders of magnitude higher than the silver-coated close-packed a-Si spheres (*i.e.*, the reference substrate), which is regarded to be analogous to silver-coated close-packed PS spheres.[10] Importantly, compared to traditional surface- or tip-enhanced Raman spectroscopy using bare metal particles or metal tips as Raman signal amplifier, MDPCs eliminate direct interaction between the metal and probed molecules by an isolated shell, which has proven to be effective in preserving original vibrational information[39,40] and providing more accurate surface Raman signals. Furthermore, MDPCs possess better performance than other substrates we prepared through the similar procedure (Supporting Information S7) or some other methods,[30,41−44] which further illustrated the importance of introducing multiple MD configurations. Lastly, the MDPCs only showed little variation of Raman enhancement after storage in ambient conditions for one month (Supporting Information S8).

## CONCLUSION

MDPCs are used as SERS substrates for ultrasensitive molecular detectors. Calculation and experiments show that the electromagnetic fields are significantly enhanced on the surface of MDPCs. The MDPCs possess uniform site enhancement distribution and are capable of quantitative analysis and detection of R6G molecules down to 10 and 1 pM level, respectively, with excellent reproducibility and stability of Raman signals. The totality of the results suggests MDPCs to be a highly promising candidates for practical SERS applications.

## METHODS

**Calculation Methods.** In our calculation, we invoke the concept of irradiance rather than the EM field. The former refers to the flow of radiant energy incident on a surface. The calculation model is based on MD structure of silver supported on amorphous silicon (a-Si), and each MD unit is composed of a silver layer with a thickness of 18 nm and a-Si layer with a thickness of 10 nm. The pump irradiance is calculated from the pump electric field and the characteristic impedance of the medium.[21] The information of medium and that of the EM field is included in pump irradiance $I_p$, which is defined as

$$I_p = \varepsilon_0 c |E_p|^2 / 2n \quad (3)$$

where $\varepsilon_0$, $c$, $n$, and $E_p$ represent electrical permittivity of free space, speed of light in free space, refractive index of medium, and pump excitation electric field in the medium, respectively. The distribution of pump electric field is calculated by transfer matrix method.[22] The material refractive indices are chosen from ref 23 for the calculation.

**Materials and Instrumentations.** The reagents are of analytical grade and used as received. The polystyrene (PS) spheres were purchased from MicroParticles GmbH. The concentration of the PS suspension is 10% (w/w), and the size distribution of the PS spheres is 978 ± 32 nm. The silicon wafer (undoped, >3000 Ωcm) was soaked in piranha solution ($H_2SO_4/H_2O_2$ 3:1 v/v) to obtain a clean surface before use. The silicon target was washed with 5% hydrofluoric acid and presputtered for 30 min before the deposition of a-Si. The scanning electron microscopy (SEM) observation was performed on a Philips XL 30 FEG SEM. The Raman spectra were collected from a Renishaw 2000 laser Raman microscope equipped with a 633 nm argon ion laser of 2 $\mu$m spot size for excitation.

**Fabrication of MDPCs.** A modified self-assembly technique[24] was used to fabricate the PS self-assembled monolayer (SAM). The PS suspension was first diluted by mixing with equal volumes of ethanol. Subsequently, the as-prepared ethanol/water PS solution was applied to form the PS SAM on the surface of the water, under which the supporting substrate was prelocated. The water was pumped out, and the monolayer was dried under ambient conditions. Afterward, the substrate with PS SAM was heated at 90 °C in vacuum for PS shrinkage and SAM mechanical enhancement. After that, the substrate was loaded in a radio frequency magnetron sputtering system for a-Si deposition. The deposition speed was ∼1.8 Å/s, and deposition time was 3 h. Then, a silver layer with a thickness of ∼18 nm was sputtered onto the a-Si PCs, followed by sputtering ∼10 nm thick a-Si. By repeating the deposition of Ag and a-Si layers, a-Si PCs with the desired numbers of MD units were fabricated. Finally, the as-obtained MDPCs were immersed in chloroform to remove the PS template. The as-fabricated MDPCs show strong and uniform diffraction colors,

and their size reaches tens of square centimeters, determined only by the size of PS SAM.

**SERS Efficiency Evaluation.** The MDPC substrate was cut into $3 \times 3$ mm$^2$ and soaked in 0.5 mL of aqueous rhodamine 6G (R6G) and 4-mercaptobenzoic acid (4-MBA) solution of different concentrations for a certain time until an adsorption/desorption equilibrium was reached. The MDPC squares were washed with distilled water several times and dried under ambient conditions before the test. The evaluation of SERS performance was carried out on a randomly chosen area of an MDPC square. The reproducibility evaluation was carried out on 30 randomly chosen areas, and the stability evaluation was carried out by measuring 15 Raman spectra on the same MDPC square every two days. In all experiments, the laser power was fixed to 25 mW, 1%, and integration time was 20 s.

*Acknowledgment.* This work was supported by Research Grants Council of Hong Kong SAR (Grant No. CityU 101807 and CityU5/CRF/08).

*Supporting Information Available:* Calculation results of normalized $I_p$, digital image of the PS SAM, SEM images of MDPCs, EF calculation, SERS intensity mapping, and Raman spectra. This material is available free of charge *via* the Internet at http://pubs.acs.org.

## REFERENCES AND NOTES


1. Jeanmaire, D. L.; Van Duyne, R. P. Surface Raman Spectroelectrochemistry Part I. Heterocyclic, Aromatic, and Aliphatic Amines Adsorbed on Anodized Silver Electrode. *J. Electroanal. Chem.* **1977,** *84*, 1–20.
2. Fleischmann, M.; Hendra, P. J.; McQuillan, A. J. Raman Spectra of Pyridine Adsorbed at a Silver Electrode. *Chem. Phys. Lett.* **1974,** *26*, 163–166.
3. Albrecht, M. G.; Creighton, J. A. Anomalously Intense Raman Spectra of Pyridine at a Silver Electrode. *J. Am. Chem. Soc.* **1977,** *99*, 5215–5217.
4. Nie, S.; Emory, S. R. Probing Single Molecules and Single Nanoparticles by Surface-Enhanced Raman Scattering. *Science* **1997,** *275*, 1102–1106.
5. Kneipp, K.; Kneipp, H.; Itzkan, I.; Dasari, R. R.; Feld, M. S. Ultrasensitive Chemical Analysis by Raman Spectroscopy. *Chem. Rev.* **1999,** *99*, 2957–2975.
6. Li, W.; Camargo, P. H. C.; Au, L.; Zhang, Q.; Rycenga, M.; Xia, Y. Etching and Dimerization: A Simple and Versatile Route to Dimers of Silver Nanospheres with a Range of Sizes. *Angew. Chem., Int. Ed.* **2010,** *49*, 164–168.
7. Mulvihill, M. J.; Ling, X. Y.; Henzie, J.; Yang, P. Anisotropic Etching of Silver Nanoparticles for Plasmonic Structures Capable of Single-Particle SERS. *J. Am. Chem. Soc.* **2010,** *132*, 268–274.
8. Lim, D.-K.; Jeon, K.-S.; Kim, H. M.; Nam, J.-M.; Suh, Y. D. Nanogap-Engineerable Raman-Active Nanodumbbells for Single-Molecule Detection. *Nat. Mater.* **2010,** *9*, 60–67.
9. Yang, M.; Alvarez-Puebla, R.; Kim, H.-S.; Aldeanueva-Potel, P.; Liz-Marzn, L. M.; Kotov, N. A. SERS-Active Gold Lace Nanoshells with Built-in Hotspots. *Nano Lett.* **2010,** *10*, 4013–4019.
10. Fang, Y.; Seong, N. H.; Dlott, D. D. Measurement of the Distribution of Site Enhancements in Surface-Enhanced Raman Scattering. *Science* **2008,** *321*, 388–392.
11. Tessier, P. M.; Velev, O. D.; Kalambur, A. T.; Rabolt, J. F.; Lenhoff, A. M.; Kaler, E. W. Assembly of Gold Nanostructured Films Templated by Colloidal Crystals and Use in Surface-Enhanced Raman Spectroscopy. *J. Am. Chem. Soc.* **2000,** *122*, 9554–9555.
12. Tian, Z.-Q.; Ren, B.; Wu, D.-Y. Surface-Enhanced Raman Scattering: From Noble to Transition Metals and from Rough Surfaces to Ordered Nanostructures. *J. Phys. Chem. B* **2002,** *106*, 9463–9483.
13. Tao, A; Sinsermsuksakul, P.; Yang, P. Tunable Plasmonic Lattices of Silver Nanocrystals. *Nat. Nanotechnol.* **2007,** *2*, 435–440.
14. Wu, D. Y.; Li, J. F.; Ren, B.; Tian, Z. Q. Electrochemical Surface-Enhanced Raman Spectroscopy of Nanostructures. *Chem. Soc. Rev.* **2008,** *37*, 1025–1041.
15. Jensen, T. R.; Duval, M. L.; Kelly, K. L.; Lazarides, A. A.; Schatz, G. C.; Van Duyne, R. P. Nanosphere Lithography: Effect of the External Dielectric Medium on the Surface Plasmon Resonance Spectrum of a Periodic Array of Silver Nanoparticles. *J. Phys. Chem. B* **1999,** *103*, 9846–9853.
16. Gonçalves, M. R.; Siegel, A.; Marti, O. SERS Observed in Periodic Metallo-Dielectric Nanostructures Fabricated Using Coated Colloidal Crystals. *Proc. SPIE* **2008,** *6988*, 698809.
17. Wang, X.; Liu, Z.; Zhuang, M. D.; Zhang, H. M.; Wang, X.; Xie, Z. X.; Wu, D. Y.; Ren, B.; Tian, Z. Q. Tip-Enhanced Raman Spectroscopy for Investigating Adsorbed Species on a Single-Crystal Surface Using Electrochemically Prepared Au Tips. *Appl. Phys. Lett.* **2007,** *91*, 101105.
18. Le, F.; Brandl, D. W.; Urzhumov, Y. A.; Wang, H.; Kundu, J.; Halas, N. J.; Aizpurua, J.; Nordlander, P. Metallic Nanoparticle Arrays: A Common Substrate for Both Surface-Enhanced Raman Scattering and Surface-Enhanced Infrared Absorption. *ACS Nano* **2008,** *2*, 707–718.
19. Bortchagovsky, E.; Klein, S.; Fischer, U. C. Surface Plasmon Mediated Tip Enhanced Raman Scattering. *Appl. Phys. Lett.* **2009,** *94*, 063118.
20. Li, S.; Pedano, M. L.; Chang, S.-H.; Mirkin, C. A.; Schatz, G. C. Gap Structure Effects on Surface-Enhanced Raman Scattering Intensities for Gold Gapped Rods. *Nano Lett.* **2010,** *10*, 1722–1727.
21. Hecht, E. *Optics*, 4th ed.; Addison-Wesley: Reading, MA, 2002.
22. Yeh, P. *Optical Waves in Layered Media*; Wiley: New York, 1988.
23. Palik, E. D. *Handbook of Optical Constants of Solids*; Academic: Orlando, FL, 1985.
24. Kosiorek, A.; Kandulski, W.; Chudzinski, P.; Kempa, K.; Giersig, M. Shadow Nanosphere Lithography: Simulation and Experiment. *Nano Lett.* **2004,** *4*, 1359–1363.
25. Lin, X. M.; Cui, Y.; Xu, Y.-H.; Ren, B.; Tian, Z.-Q. Surface-Enhanced Raman Spectroscopy: Substrate-Related Issues. *Anal. Bioanal. Chem.* **2009,** *394*, 1729–1745.
26. Lu, Y.; Liu, G. L.; Lee, L. P. High-Density Silver Nanoparticle Film with Temperature-Controllable Interparticle Spacing for a Tunable Surface Enhanced Raman Scattering Substrate. *Nano Lett.* **2005,** *5*, 5–9.
27. Schmidt, J. P.; Cross, S. E.; Buratto, S. K. Surface-Enhanced Raman Scattering from Ordered Ag Nanocluster Arrays. *J. Chem. Phys.* **2003,** *121*, 10657–10659.
28. Lu, L.; Eychmüller, A.; Kobayashi, A.; Hirano, Y.; Yoshida, K.; Kikkawa, Y.; Tawa, K.; Ozaki, Y. Designed Fabrication of Ordered Porous Au/Ag Nanostructured Films for Surface-Enhanced Raman Scattering Substrates. *Langmuir* **2006,** *22*, 2605–2609.
29. Cui, B.; Clime, L.; Li, K.; Veres, T. Fabrication of Large Area Nanoprism Arrays and Their Application for Surface Enhanced Raman Spectroscopy. *Nanotechnology* **2008,** *19*, 145302.
30. Choi, D.; Choi, Y.; Hong, S.; Kang, T.; Lee, L. P. Self-Organized Hexagonal-Nanopore SERS Array. *Small* **2010,** *6*, 1741–1744.
31. Kneipp, K. High-Sensitive SERS on Colloidal Silver Particles in Aqueous Solution. *Exp. Techn. Phys.* **1988,** *36*, 161.
32. Rodger, C.; Smith, W. E.; Dent, G.; Edmondson, M. Surface-Enhanced Resonance-Raman Scattering: An Informative Probe of Surfaces. *J. Chem. Soc., Dalton Trans.* **1996,** *1996*, 791–799.
33. Zeisel, D.; Deckert, V.; Zenobi, R.; Vo-Dinh, T. Near-Field Surface-Enhanced Raman Spectroscopy of Dye Molecules Adsorbed on Silver Island Films. *Chem. Phys. Lett.* **1998,** *283*, 381–385.
34. McFarland, A. D.; Young, M. A.; Dieringer, J. A.; Van Duyne, R. P. Wavelength-Scanned Surface-Enhanced Raman Excitation Spectroscopy. *J. Phys. Chem. B* **2005,** *109*, 11279–11285.
35. Natan, M. J. Surface Enhanced Raman Scattering. *Faraday Discuss.* **2006,** *132*, 321–328.
36. Orendorff, C. J.; Gole, A.; Sau, T. K.; Murphy, C. J. Surface-Enhanced Raman Spectroscopy of Self-Assembled Monolayers: Sandwich Architecture and Nanoparticle Shape Dependence. *Anal. Chem.* **2005,** *77*, 3261–3266.

37. Gao, S.; Zhang, H.; Wang, X.; Yang, J.; Zhou, L.; Peng, C.; Sun, D.; Li, M. Unique Gold Sponges: Biopolymer-Assisted Hydrothermal Synthesis and Potential Application as Surface-Enhanced Raman Scattering Substrates. *Nanotechnology* **2005,** *16*, 2530–2535.
38. He, D.; Hu, B.; Yao, Q.-F.; Wang, K.; Yu, S.-H. Large-Scale Synthesis of Flexible Free-Standing SERS Substrates with High Sensitivity: Electrospun PVA Nanofibers Embedded with Controlled Alignment of Silver Nanoparticles. *ACS Nano* **2009,** *3*, 3993–4002.
39. Li, J. F.; Huang, Y. F.; Ding, Y.; Yang, Z. L.; Li, S. B.; Zhou, X. S.; Fan, F. R.; Zhang, W.; Zhou, Z. Y.; Wu, D. Y.; *et al.* Shell-Isolated Nanoparticle-Enhanced Raman Spectroscopy. *Nature* **2010,** *464*, 392–395.
40. Liu, Y.-C.; Yu, C.-C.; Hsu, T. C. Improved Performances on Surface-Enhanced Raman Scattering Based on Electrochemically Roughened Gold Substrates Modified with $SiO_2$ Nanoparticles. *J. Raman Spectrosc.* **2009,** *40*, 1682–1686.
41. Baia, M.; Baia, L.; Astilean, S. Gold Nanostructured Films Deposited on Polystyrene Colloidal Crystal Templates for Surface-Enhanced Raman Spectroscopy. *Chem. Phys. Lett.* **2005,** *404*, 3–8.
42. Lu, L.; Randjelovic, I.; Capek, R.; Gaponik, N.; Yang, J.; Zhang, H.; Eychmüller, A. Controlled Fabrication of Gold-Coated 3D Ordered Colloidal Crystal Films and Their Application in Surface-Enhanced Raman Spectroscopy. *Chem. Mater.* **2005,** *17*, 5731–5736.
43. Luo, L.-B.; Chen, L.-M.; Zhang, M.-L.; He, Z.-B.; Zhang, W. F.; Yuan, G.-D.; Zhang, W.-J.; Lee, S.-T. Surface-Enhanced Raman Scattering from Uniform Gold and Silver Nanoparticle-Coated Substrates. *J. Phys. Chem. C* **2009,** *113*, 9191–9196.
44. Huang, Z.; Meng, G.; Huang, Q.; Yang, Y.; Zhu, C.; Tang, C. Improved SERS Performance from Au Nanopillar Arrays by Abridging the Pillar Tip Spacing by Ag Sputtering. *Adv. Mater.* **2010,** *22*, 4136–4139.